Correction of color information of a 3D model using a range intensity image

Megumi Shinozaki [a], Masato Kusanagi [a], Kazunori Umeda [a,*], Guy Godin [b], Marc Rioux [b]

[a] *Faculty of Science and Engineering, Department of Precision Mechanics, Chuo Univ., 1-13-27 Kasuga, Bunkyo-ku, Japan*
[b] *Visual Information Technology Group, National Research Council, Canada*

ARTICLE INFO

ABSTRACT

Most active optical range sensors record, simultaneously with the range image, the amount of light reflected at each measured surface location: this information forms what is called a range intensity image, also known as a reflectance image. This paper proposes a method that uses this type of image for the correction of the color information of a textured 3D model. This color information is usually obtained from color images acquired using a digital camera. The lighting condition for the color images are usually not controlled, thus this color information may not be accurate. On the other hand, the illumination condition for the range intensity image is known since it is obtained from a controlled lighting and observation configuration, as required for the purpose of active optical range measurement. The paper describes a method for combining the two sources of information, towards the goal of compensating for a reference range intensity image is first obtained by considering factors such as sensor properties, or distance and relative surface orientation of the measured surface. The color image of the corresponding surface portion is then corrected using this reference range intensity image. A B-spline interpolation technique is applied to reduce the noise of range intensity images. Finally, a method for the estimation of the illumination color is applied to compensate for the light source color. Experiments show the effectiveness of the correction method using range intensity images.

© 2009 Elsevier Inc. All rights reserved.

1. Introduction

Constructing textured three-dimensional (3D) models of real objects is an important issue in the field of computer vision. The texture mapping technique [1] using color images captured by a digital camera is often used for creating a realistic 3D model. However, the illumination under which color images are captured cannot usually be controlled, and thus the color information is affected by the illumination. There are several approaches to address this problem. Some methods actually control lighting conditions for the purpose of measuring reflectance properties, e.g. [2–4]. Ikeuchi and Sato [2] measure reflectance properties with a range image and a brightness image. Kay and Caelli [3] reconstruct reflectance properties from one range image and four or more color images under different point light sources. Sato et al. [4] acquire multiple range and color images by rotating an object and construct a whole 3D model with complex texture. In these methods, a Torrance–Sparrow model [5] is modified and used to separate diffuse and specular components and recover reflectance properties. Bernardini and Rushmeier [6] present a broad survey of techniques for 3D model acquisition including reflectance properties. Tominaga and Tanaka [7] and Tan et al. [8] separate the diffuse and specular components from a color image.

An active range sensor measures distance by projecting light (laser or incoherent) onto a surface and measuring a property of the reflected light (triangulation angle, time-of-flight, etc.). The amount of reflected light is a function of the reflectance properties of the measured surface point. The array of the measured power produces an intensity image with the same sampling pattern as the geometric component of the range image. This is called a *range intensity image* or a *reflectance image*. Hereafter, this paper uses the term *range intensity image*. The use of range intensity images for registration of a range image and a color image has been successfully demonstrated before [9–13].

In this paper, we focus on another useful feature of a range intensity image [14,15]. The lighting condition yielding the range intensity image is controlled since this image is taken under known lighting conditions by virtue of the geometric sensing process. This paper investigates the application of a range intensity image to the correction of the color information of a colored 3D model. The goal is to exploit the respective advantages of a range intensity image and a color image. The controlled sensing geometry on both the illumination and observation sides, combined with the measured surface geometry, allows the inversion of an illumination model and the derivation of a corrected range intensity image representing the intrinsic reflectance properties of the surface. Using the corrected value of the range intensity image, we can adjust the intensity level of the color image. By conforming the value of the color image to that of the range intensity image, the proper

* Corresponding author. Fax: +81 3 3817 1820.
E-mail address: umeda@mech.chuo-u.ac.jp (K. Umeda).

intensity level is obtained without estimating the illumination for the color image. Additionally, we introduce the method to estimate the illumination color proposed by Lehmann and Palm [16], and compensate for the chromatic properties of the illuminant.

This paper is organized as follows. In Section 2, we explain the characteristics of a range intensity image and show the flow of the correction method. In Section 3, we describe the method for correcting the intensity of a color image using a range intensity image. After introducing the method to estimate the illumination color in Section 4, we show several experimental results in Section 5, and then we conclude the paper in Section 6.

## 2. Outline of the correction method

2.1. Characteristics of a range intensity image

Fig. 1 shows an example of a range intensity image and a color image of the same object. A range intensity image is monochrome (with some exceptions such as [17]) while a color image contains multiple channels, usually red, green and blue. Thanks to sustained advances in the resolution of off-the-shelf digital cameras, a typical color image is denser than a range intensity image. Additionally, a color image usually exhibits a better S/N (signal-to-noise) ratio. Fig. 2 shows cross-sections of a the red channel of a color image and of a range intensity image for a white and flat surface. They were acquired using the experimental system described later. The difference of S/N ratios is obvious. One cause is the effect of laser speckle [18]. Nevertheless, a range intensity image can be useful because, as indicated above, its illumination geometry and power can be controlled at capture time, and thus it can serve in the estimation of surface reflectance properties. Table 1 summarizes the comparison of characteristics between a color and a range intensity image.

2.2. Flow of the correction method

Fig. 3 illustrates the flow of the correction method. In the first step, a reference range intensity image without shading and highlights is obtained. Secondly, the reference range intensity image is projected onto the color image plane. The ratio between the range intensity value and the color value at each corresponding point is computed. Then, correction of intensities of the entire color image is achieved by multiplying the RGB values by the ratio values interpolated at each point of the color image. Finally, the illumination color is compensated by applying the method of [16].

We assume that a range intensity image is not affected by ambient light, and that light sources for a color image are composed of a uniform color.
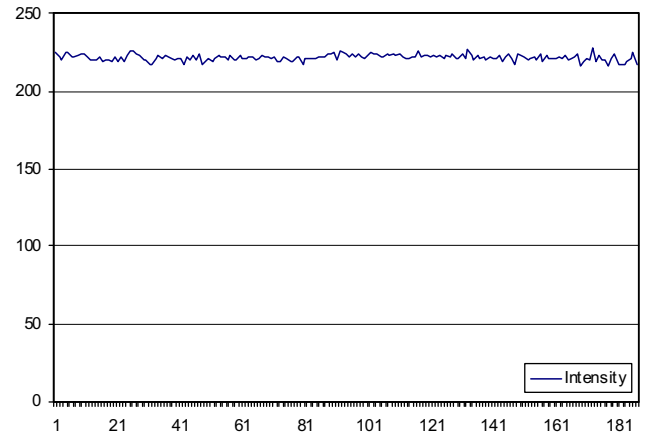
(a)Color image
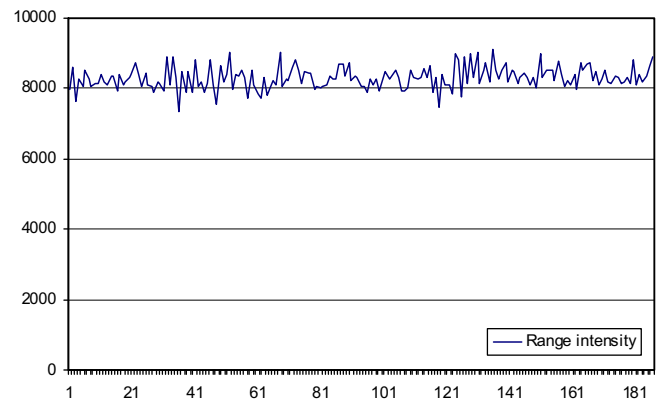
(b)Range intensity image

Fig. 2. Comparison of S/N ratio between color and range intensity images. Range intensity image has lower S/N ratio.

Table 1
Comparison of color and range intensity images.

	Color image	Range intensity image
Color	RGB	Intensity only
Resolution	High	Low to medium
S/N ratio	High	Low
Illumination	Unknown	Controlled

(a)Color image

(b)Range intensity image

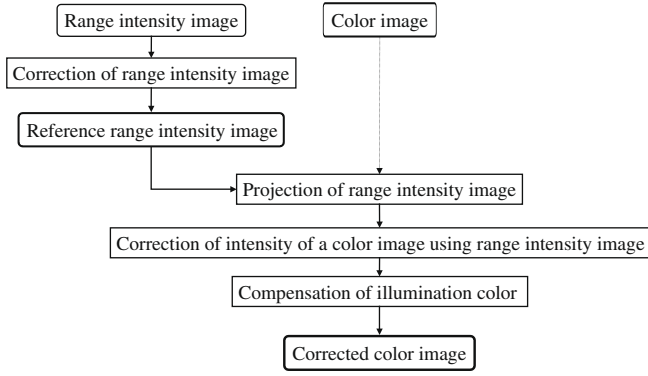**Fig. 1.** Comparison of color and range intensity images. The main differences between the two are summarized in Table 1.

Fig. 3. Flowchart of the correction method.

3. Correction of intensity of a color image

3.1. Reference range intensity image

The first step in the correction of a color image from a range intensity image requires the estimation of a reference range intensity image. A range intensity image is affected by the following factors [19]:

- Distance to each measured point
- Normal vector at the measured point
- Sensor-specific characteristics
- Reflectance properties of the illuminated surface

Attenuation due to distance has an inverse-of-square effect on the range intensity values. Normal vectors can be estimated from the range measurements, and can be used in the inversion of a reflectance model. Generally, the range intensity values are proportional to the cosine of the incident angle of the active lighting. Sensor-specific characteristics have to be calibrated individually: these include the imaging geometry (incidence and observation), and the sensor's response as a function of incident power, expressed here as a gamma characteristic. Considering these factors, the range intensity value I_{obs} observed by the sensor can be represented by

$$I_{obs} = \left\{ k(l) \frac{\cos \theta}{l^2} I \right\}^{\gamma} \tag{1}$$

where γ is the gamma value and $k(l)$ is a function that represents the variation in sensitivity of each sensor unit. From this equation, we can estimate the range intensity value I without the influence of these factors.

According to the dichromatic reflection model [20], the range intensity values contain diffuse and specular components. Torrance–Sparrow model [5] is often used as the dichromatic reflection model. In Fig. 4, the specular component is the function of
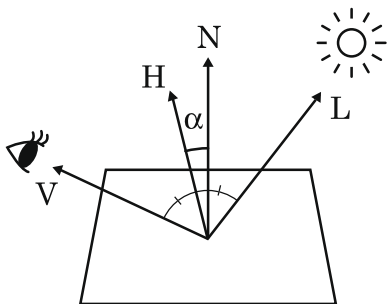
the angle between the normal vector (N) and the bisector (H) of directions to the lighting (L) and the camera (V).

We simplify the Torrance–Sparrow model and use the following equation as the reflectance model:

$$I = I_d \left\{ 1 + k \exp \left(-\frac{\alpha^2}{2\sigma^2} \right) \right\} \tag{2}$$

where k is a coefficient that weighs the portion of the specular component, i.e., the maximum ratio of the specular reflectance to the diffuse reflectance, and σ is a coefficient representing the roughness of the surface. This model is based on the strong assumption that the ratio of the diffuse and specular components is constant regardless of the intensity. We do not discuss the validity of this assumption in detail in this paper. Under this assumption, the diffuse component I_d can be easily obtained by dividing the intensity I by the term after I_d, when k and σ are given and α is measured. We use I_d for the reference range intensity image.

3.2. Correction of intensity of a color image

Once a reference range intensity image is obtained, it can be used as the basis for correcting a color image, since its represents an estimate of the diffuse reflectance coefficient in the wavelength of the range sensing system. We propose a procedure to correct the intensity of a color image as follows.

(1) *Projection of range intensity image.* The corrected range intensity image is projected onto the color image, following registration of the two images using the method given in [13] which provides the intrinsic and extrinsic parameters between the range image and the color image with a gradient-based method. Fig. 5 illustrates this projection. The projected points of the range intensity image are in general sparser and not aligned with the color image pixels.

(2) *Acquisition of color value at each range intensity image pixel.* The color image's color value at each range intensity image pixel can be obtained by an interpolation technique. Using a bilinear interpolation, the color value is calculated using four surrounding color image pixels.

(3) *Calculation of the ratio at each range intensity image pixel.* The ratio between the range intensity value I_{ri} and the color value I_c is obtained as $c = I_{ri}/I_c$. The color image usually consists of R, G and B channels: the one that is the closest in

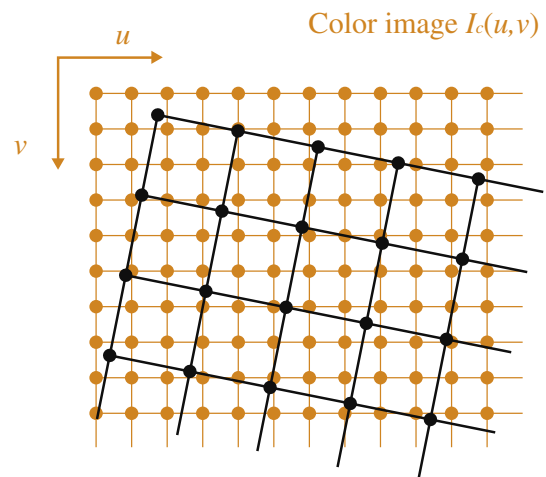Fig. 4. Parameters for Torrance–Sparrow model.

Fig. 5. Projection of a range intensity image on a color image. The projected points of the range intensity image are sparser and not aligned with color image pixels.

color to the range sensor's light is used. Notice that the two images should be normalized beforehand in order to adjust the dynamic range of the two images.

(4) *Calculation of the ratio at each color image pixel.* Once the ratio at the locus of each point of the range intensity image is obtained, it is necessary to interpolate the ratio at each point of the color image. In this paper, we adopt a B-spline surface fitting interpolation approach. With this interpolation, the effect of the poor S/N ratio of range intensity images (see Fig. 2) is reduced.

The B-spline surface is a parametric surface which generates a mathematically smooth surface. A non-rational B-spline surface is defined as follows [21]:

$$\mathbf{P}(u,v) = \sum_{i=0}^{n_u-1} \sum_{j=0}^{n_v-1} N_{i,m_u}(u) N_{j,m_v}(v) \mathbf{q}_{ij} \tag{3}$$

where $\mathbf{q}_{ij}$ is a control net (provided as the original dataset) and $N_{i,m_u}(u)$ and $N_{j,m_v}(v)$ are the normalized B-spline basis functions of degree m_u and m_v in the u and v directions, respectively. Increasing the degree makes the surface smooth. The maximum degree is the same as the number of control points in the u and v directions. Several methods exist for the computation of the normalized B-spline basis functions. In this paper, we adopt the de Boor–Cox algorithm as follows:

$$
\begin{aligned}
N_{i,1}(u) &= \begin{cases} 1 & u_i \leqslant u < u_{i+1} \\ 0 & u < u_i, u_{i+1} \leqslant u \end{cases}. \\
N_{i,m_u}(u) &= \frac{u - u_i}{u_{i+m_u} - u_i} N_{i,m_u-1}(u) + \frac{u_{i+m_u} - u}{u_{i+m_u} - u_{i+1}} N_{i+1,m_u-1}(u) \\
N_{j,1}(v) &= \begin{cases} 1 & v_j \leqslant v < v_{j+1} \\ 0 & v < v_j, v_{j+1} \leqslant v \end{cases}. \\
N_{j,m_v}(v) &= \frac{v - v_j}{v_{j+m_v} - v_j} N_{j,m_v-1}(v) + \frac{v_{j+m_v} - v}{v_{j+m_v} - v_{j+1}} N_{j+1,m_v-1}(v)
\end{aligned}
\tag{4}
$$

u_i, v_j are components of knot vectors:

$$\mathbf{U} = [u_0, u_1, \ldots, u_{m_u+n_u+1}], \quad \mathbf{V} = [v_0, v_1, \ldots, v_{m_v+n_v+1}]$$

We define a 3D space which consists of the image plane (u, v) in Fig. 5 and the correction-coefficient axis in the direction perpendicular to the image plane.

A B-spline surface is fitted to the points where the ratio of the range intensity image is known. The value of the fitted surface at each pixel coordinate of the color image yields the interpolated ratio. In this process, a segmented area which consists of $n_u \times n_v$ points of the range intensity image is used as the control net.

(5) *Correction of the color image.* The RGB values of each point are corrected by the calculated ratio. Note that the same ratio is applied to the R, G, and B values.

In effect, the proposed procedure applies a low-pass filter to the ratio data by fitting a B-spline surface to attenuate the lower S/N ratio of range intensity images. Ratio data, which are produced by the difference of illumination conditions of range intensity and color images, do not contain high-frequency components when the illumination conditions under which the color image was captured are not complex. Therefore, given the other limitations of this recovery technique, this low-pass filtering, on the ratios but not on the color content, does not have a major impact on the appearance of the color image, which we think is the advantage of the proposed procedure.
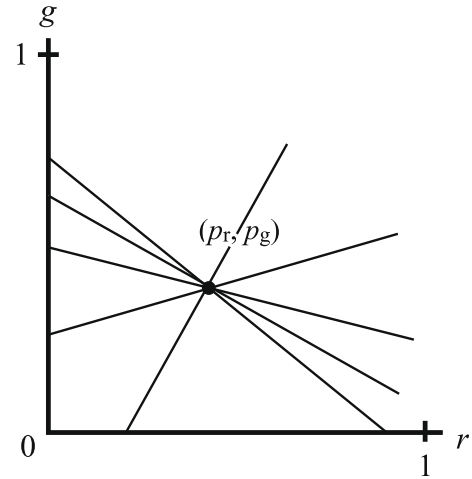

Fig. 6. Intersection of color lines.

4. Estimation of illumination color

4.1. Underlying principle

We briefly introduce the method of Lehmann and Palm [16] for the estimation of the illumination color.

Color vector of an RGB image is expressed as follows with the dichromatic reflection model.

$$
\begin{pmatrix} R \\ G \\ B \end{pmatrix} = w_d \begin{pmatrix} \beta_d^R s^R \\ \beta_d^G s^G \\ \beta_d^B s^B \end{pmatrix} + w_s \beta_s \begin{pmatrix} s^R \\ s^G \\ s^B \end{pmatrix}
\tag{5}
$$

The first and second terms represent diffuse and specular components, respectively. w_d and w_s are the weights for diffuse and specular reflections that are defined geometrically, β_d and β_s are the diffuse and specular reflectance terms, respectively, and $(s^R, s^G, s^B)^T$ represents the RGB components of the incident light. The illumination color is estimated by obtaining $(s^R, s^G, s^B)^T$ in (5), assuming that a specular reflection bears the color of the incident light.

Let the normalized color r, g for RGB color space as

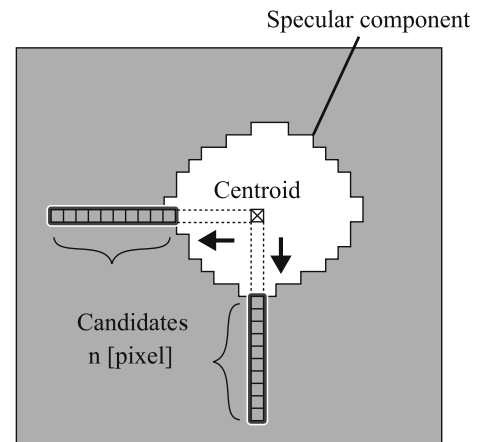$$r = \frac{R}{R+G+B}, \quad g = \frac{G}{R+G+B} \tag{6}$$

Fig. 7. Flow of selection of candidates for color lines.

Fig. 8. ShapeGrabber range sensor with a target object.

A region of a same color that contains a specular reflection forms a line (color line) in the rg space. When multiple color regions are plotted, these lines intersect at a point in rg space as illustrated in Fig. 6. The illumination color is estimated as the coordinates of the point. The line equation is obtained as follows by substituting (5) for (6).

$$g = a'r + b' \tag{7}$$

$$a' = -\frac{1 - \frac{s^B(\beta_d^B - \beta_d^G)}{s^R(\beta_d^G - \beta_d^R)}}{1 + \frac{s^B(\beta_d^B - \beta_d^R)}{s^G(\beta_d^G - \beta_d^R)}}, \quad b' = \frac{1}{1 + \frac{s^B(\beta_d^B - \beta_d^R)}{s^G(\beta_d^G - \beta_d^R)}}$$

As shown in (7), a' and b' are defined by the incident light $(s^R, s^G, s^B)^T$ and the diffuse reflectance $(\beta_d^R, \beta_d^G, \beta_d^B)^T$ only. Every line passes through the point (p_r, p_g),

$$p_r = \frac{s^R}{s^R + s^G + s^B}, \quad p_g = \frac{s^G}{s^R + s^G + s^B} \tag{8}$$

When (p_r, p_g) is obtained, the illumination color $(s^R, s^G, s^B)^T$ can be calculated with (8).

4.2. Estimation of illumination color

We extract color lines around regions with strong specular reflection. Firstly, we identify regions with high intensities by thresholding and obtain the centroid of each region. As the ratio of the range intensity value to the color value is obtained at each color image pixel, we can threshold not only on the basis of intensity itself but also of the ratio. Then we investigate the intensities along specific directions (chosen here as leftward and downward) and choose n pixels out of the thresholded region as shown in Fig. 7.

We calculate r, g of each pixel and then obtain a color line by applying the least-squares method for the n pixels. When color lines are obtained for every region with specular reflection, we obtain the intersection point (p_r, p_g) with the least-squares method. The ratio of the components of the illumination color $(s^R, s^G, s^B)^T$ is given by $(p_r, p_g, 1 - p_r - p_g)^T$.

Finally, we compensate the obtained illumination color, and modify the color with the following equation.

$$\begin{pmatrix} R_{new} \\ G_{new} \\ B_{new} \end{pmatrix} = \begin{pmatrix} \frac{p_g}{p_r}R \\ G \\ \frac{p_g}{1-p_r-p_g}B \end{pmatrix} \tag{9}$$

5. Experiments

5.1. Range image sensor

The range image sensor used for the experiments is the Shape-Grabber system, with a scan head SG-100 on a PLM300 linear displacement mechanism [22]. It projects a slit of laser light and measures distances by triangulation. The number of points mea-
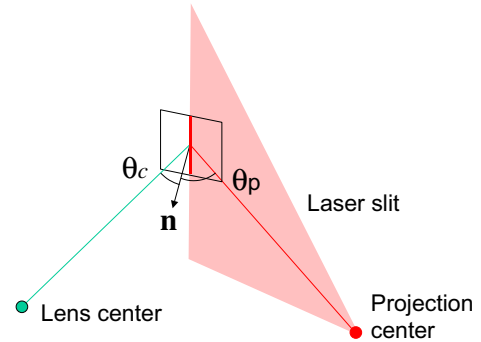

Fig. 10. Imaging angle for the ShapeGrabber range sensor. The range intensity values are observed to be proportional to $cos\theta_c$, not to $cos\theta_p$.
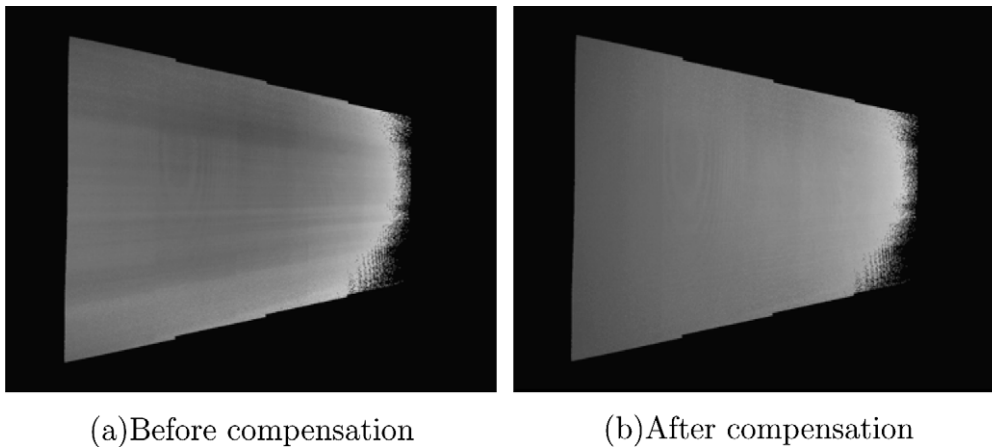

Fig. 9. Compensation of each sensor element. (a) Original image of a slanted plane with gamma correction, (b) after compensation of variance of each element's sensitivity. Variance of each element's sensitivity is compensated.
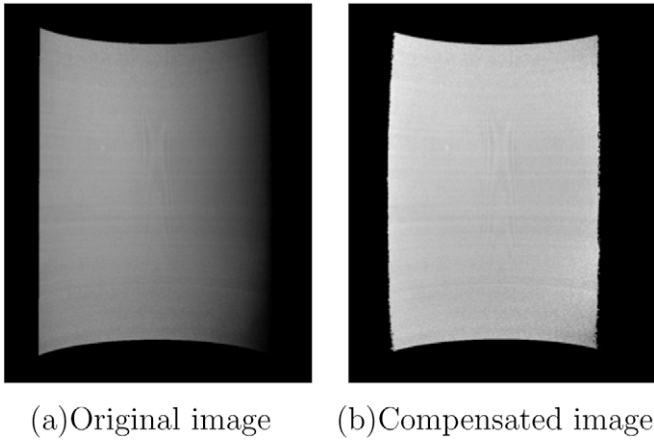
(a)Original image   (b)Compensated image

Fig. 11. Compensation of normal vector: vertical cylinder. The shading caused by the surface slant removed and the image becomes flat.

sured along each slit is 1280. The number of measurements in the other direction is a function of the mechanical displacement. The system provides a range intensity image along with the range data. Fig. 8 shows the ShapeGrabber sensor with a target object. The left box is a laser slit projector, and the right larger box is a CCD camera. The upper part is the linear displacement system.

5.1.1. Sensor characteristics for intensity measurement

We determined experimentally that the gamma value of the camera was not equal to 1: the estimated value was around 0.45.

The sensor also shows some variation in sensitivity for each element, as shown in Fig. 9(a). This figure shows the juxtaposition of four range intensity images for a slanted plane. The reason for this fluctuation most likely results from the non-uniformity of the laser slit and the vignetting effect of the lens in the CCD camera. Using experimental data, we applied compensation by 2nd order polynomial for every 1280 elements. Fig. 9(b) illustrates the results of this compensation.
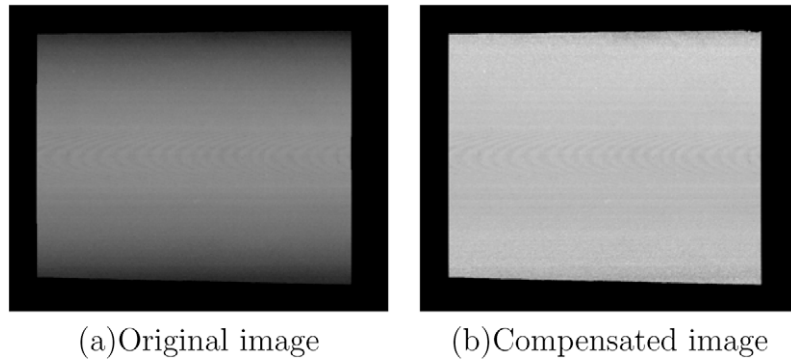

(a)Original image   (b)Compensated image

Fig. 12. Compensation of normal vector: horizontal cylinder. The shading caused by the surface slant removed and the image becomes flat.
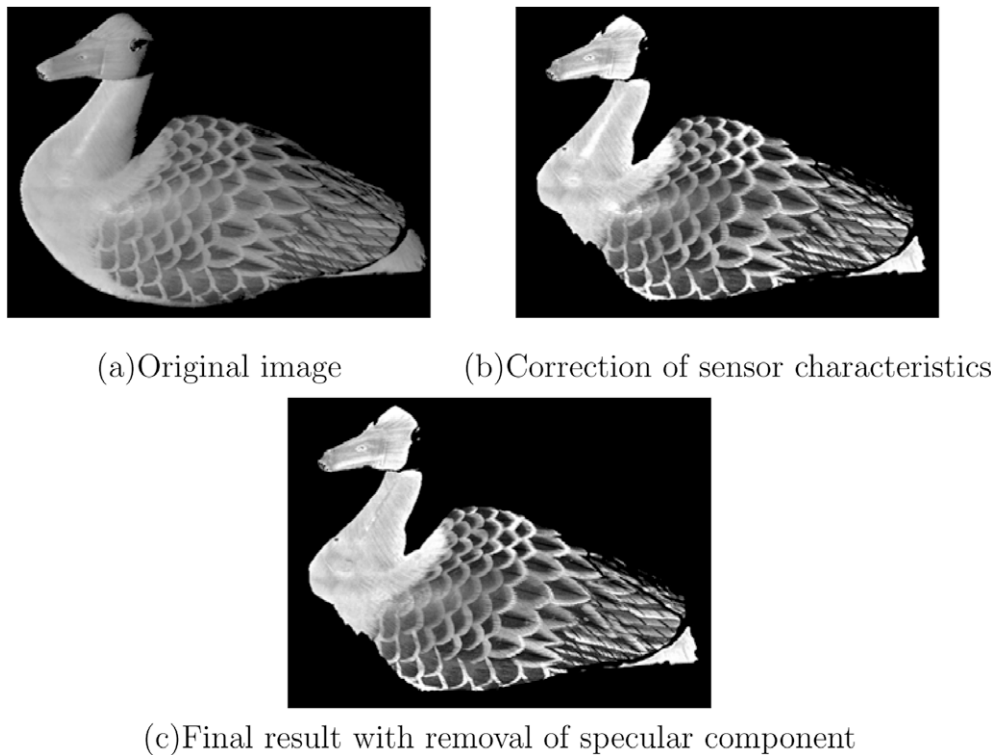

(a)Original image   (b)Correction of sensor characteristics

(c)Final result with removal of specular component

Fig. 13. Correction of range intensity image.

It is interesting to note that the range intensity values are observed to be not proportional to $\cos\theta_p$, but in fact to $\cos\theta_c$ in Fig. 10.

Considering every factor mentioned above, Eq. (1) for the sensor is given as follows.

$$I_{obs} = \left\{ k(l_c) \frac{\cos\theta_c}{l_p l_c} I \right\}^{0.45}, \quad k(l_c) = al_c^2 + bl_c + c \tag{10}$$

The term l^2 in (1) is changed to $l_p l_c$, which are distances from the projector's center and from the lens center, respectively. The coefficients a, b, c are obtained for each sensor element.

Figs. 11 and 12 confirm the above sensor model: after the compensation, shading caused by the surface slant is removed and both cylinders look nearly flat.

5.2. Correction of a color image

Fig. 13(a) shows a range intensity image of a duck model with the dimensions of $148 \times 69 \times h110$ [mm³]. The range image contains 312,730 points.

The correction of gamma and sensor elements' sensitivity was first applied to the original range intensity image; then the effect of distance and normal vector was compensated.

Fig. 13(b) shows the range intensity image compensated by (10). The removed regions indicate the regions with a large slant in the left direction. With such a slant, the range intensity image

values did not obey the corrected equation, and thus they were thresholded. We can see that a uniform range intensity image is obtained overall, except for the specular components at the neck and front body, and for some peripheral regions.

Fig. 13(c) shows the result of removing the specular component with (2). We assumed that k and σ are uniform over the object, and determined them empirically as 0.4 and 0.06, respectively. It is shown that although the model of the reflectance is a simplified one, the specular components are removed for the most part.

We show the results of the correction of the intensity of color image in Fig. 14. The corrected range intensity image in Fig. 13(c) was used to correct Fig. 14(a). A Nikon COOLPIX5000 digital camera was used to capture the color image. The acquisition format was set to RAW. The size of the color image is 2560×1920. As the laser's color is red, the R-channel of the color image is used for registration and calculation of the correction coefficient. The result is Fig. 14(b). We can see that the shading and specular components have essentially disappeared. Moreover, we can observe the effectiveness of the B-spline surface fitting in the magnified images of Fig. 15. The parameters of the B-spline surface n_u, n_v, m_u, m_v were all set to 12 empirically. The effectiveness is obvious when comparing Fig. 15(a) (with bilinear interpolation) and Fig. 15(b) (with B-spline surface fitting). Fig. 15(a) shows some jaggies due to the bilinear interpolation. In contrast, we observe a smooth interpolation in Fig. 15(b).

(a)Original image

(b)Final result with color correction

Fig. 14. Correction of color image. Darker regions in the original color image such as on the bottom become uniform in the corrected image.

(a)with bilinear interpolation

(b)with B-spline surface interpolation

Fig. 15. Effect of B-spline surface fitting.

5.3. Estimation of illumination color

We show results of applying the entire procedure to a bird model with the dimensions of $150 \times 70 \times h130$ [mm³]. The model appears in Fig. 8.

Fig. 16(a) is the measured range intensity image and Fig. 16(b) is the resulting reference range intensity image. Shading is mostly removed and a uniform image is obtained in Fig. 16(b). We assumed that k and σ are uniform over the object, and determined them empirically as 0.714 and 0.068, respectively.

Figs. 17–19 show the results of correcting the intensity of color images and compensate for the effect of illumination colors. Figs. 17–19(a) are original color images captured under CIE D65, CWF, and INC A illuminations, respectively. A Gretag-Macbeth Judge II was used to produce the standard illuminations. Color temperatures of CIE D65, CWF, and INC A are 6500 K, 4150 K, and 2850 K, respectively. A Nikon D70 digital camera was used to capture the color images. Figs. 17–19(b) are the corrected images.

In Figs. 17(b) and 18(b), colors of highlights are nearly gray, and the color of whole images are well corrected. In Fig. 19(b), the correction is too bluish. This is because the illumination condition of INC A is far from the standard one and the color correction became excessive because of the errors.

Table 2 shows the estimated illumination color (r, g, b). The reference values were measured by capturing images of a gray-scale chart under each illumination. Table 2 shows that estimation of illumination color is successful, although some errors occur.

Additionally, we compared corrected color images under different illumination conditions; CIE D65, CWF, and INC A, which correspond to Figs. 17–19, respectively. Table 3 shows that the results. Each cell gives the RMS errors of (r, g) values (see (6)) between color images under two illumination conditions. Each row corre-

(a)Original color image

(b)Corrected color image

Fig. 17. Correction of color (CIE D65).
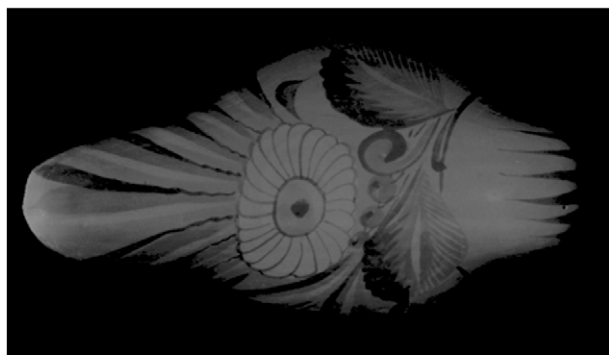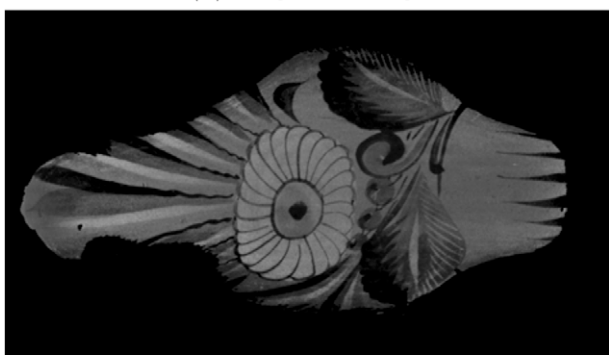
(a)Original image

(b)Corrected range intensity image

Fig. 16. Reference range intensity image of a bird model.

sponds to the kind of correction factors; original image (without correction), intensity only, intensity and estimated color, and intensity and measured color using a gray-scale chart. Values in Table 2 were used as estimated and measured color. It is shown that the error becomes smaller for every pair of illumination conditions with the proposed method to correct intensity and color. Additionally, the errors when estimated color and measured color are used for correction are comparable, which means that estimation of color with the proposed method works well. Furthermore, we tested standard illumination color values for CIE D65 and INC A comparison. The standard values of (r, g, b) are (0.2838, 0.3486, 0.3676) (CIE D65) and (0.5526, 0.3212, 0.1262) (INC A). The RMS errors were (0.1100, 0.0327). This is also comparable to the result with the proposed method (0.1285, 0.0332).

We also compared the corrected color images with correction of intensity and estimated color, and with intensity and measured color for each illumination condition. The results were (0.0399, 0.0160) (D65), (0.0046, 0.0033) (CWF), and (0.0314, 0.0767) (INC A). In each case, the value is small, which verifies again that estimation of illumination color with the proposed method works well.

Table 4 shows the correlation of corrected images with different illumination conditions. Correlation coefficients for R, G, B channels are shown. We see that the correlation becomes larger with the correction of intensity, which verifies that the proposed method to correct intensity works well. Correction of color has small effect, since the correlation is calculated for each color channel. The

(a)Original color image

(a)Original color image
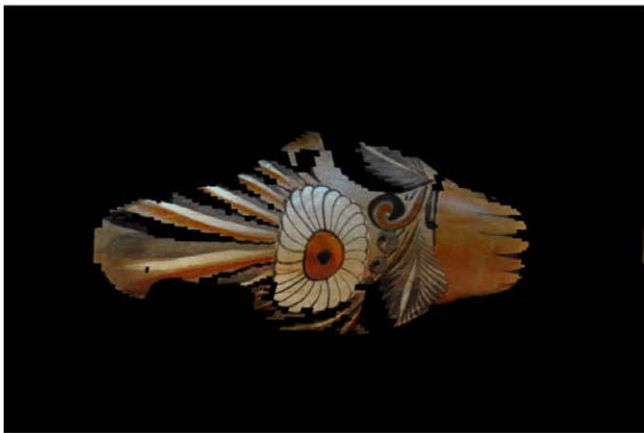
(b)Corrected color image

Fig. 18. Correction of color (CWF).

(b)Corrected color image

Fig. 19. Correction of color (INC A).

shape of lamps for CIE D65 and CWF was similar, and this is why correlation without correction of intensity between CIE D65 and CWF is relatively large.

6. Conclusion

We have proposed a method that uses the range intensity image in order to improve the color information of 3D models, by taking advantage of the fact that the lighting condition for the range intensity image is controlled as part of active range sensing. We first discussed the correction of the range intensity image itself, considering the sensor-specific factors, distance, normal vectors, etc. We then proposed a method for the correction of the intensity of a color image using the corrected range intensity image. B-spline interpolation was applied to cope with the low S/N ratio of range intensity images. We finally applied a method for the estimation of the illuminant color, and its compensation. Experiments showed the effectiveness of the proposed correction methods using range intensity images and compensation of illumination color.

In future work, we intend to improve the separation of specular components of a range intensity image and construct a method to correct color at specular regions. We are now working on improving the model of (2). The key idea is to modify the relation between the specular and the diffuse reflectance, which is now modeled as being strictly proportional. At the same time, a method to determine reflectance model parameters should be developed.

Table 2
Estimation of illumination color (r, g, b).

Name	Estimated	Measured	Errors
CIE D65	(0.357, 0.341, 0.302)	(0.319, 0.354, 0.327)	(0.038, −0.013, −0.025)
CWF	(0.444, 0.327, 0.229)	(0.439, 0.324, 0.237)	(0.005, 0.003, −0.008)
INC A	(0.602, 0.297, 0.101)	(0.633, 0.240, 0.127)	(−0.031, 0.057, −0.026)

Table 3
RMS errors (r, g) between color images under two illumination conditions.

Correction factors	D65-CWF	CWF-INC A	D65-INC A
Without correction	(0.1387, 0.0306)	(0.1618, 0.0624)	(0.2937, 0.0894)
Intensity	(0.1401, 0.0309)	(0.1609, 0.0586)	(0.2926, 0.0852)
Intensity + color	(0.0713, 0.0169)	(0.0866, 0.0282)	(0.1285, 0.0332)
Intensity + measured color	(0.0493, 0.0299)	(0.0698, 0.0781)	(0.0886, 0.0988)

Table 4
Correlation coefficients (R, G, B) of color images under two illumination conditions.

Correction factors	D65-CWF	CWF-INC A	D65-INC A
Without correction	(0.907, 0.920, 0.906)	(0.711, 0.789, 0.735)	(0.768, 0.877, 0.803)
Intensity	(0.953, 0.945, 0.916)	(0.967, 0.938, 0.871)	(0.952, 0.924, 0.836)
Intensity + color	(0.953, 0.945, 0.917)	(0.969, 0.938, 0.871)	(0.952, 0.924, 0.836)

References

[1] J.F. Blinn, M.E. Newell, Texture and reflection in computer generated images, Communications of the ACM 19 (10) (1976) 542–547.

[2] K. Ikeuchi, K. Sato, Determining reflectance properties of an object using range and brightness images, IEEE Transactions on Pattern Analysis and Machine Intelligence 13 (11) (1991) 1139–1153.

[3] G. Kay, T. Caelli, Inverting an illumination model from range and intensity maps, CVGIP: Image Understanding 59 (2) (1994) 183–201.

[4] Y. Sato, M.D. Wheeler, K. Ikeuchi, Object shape and reflectance modeling from observation, in: Proc. SIGGRAPH, vol. 97, 1997, pp. 379–387.

[5] K.E. Torrance, E.M. Sparrow, Theory of off-specular reflection from roughened surfaces, Journal of the Optical Society of America 57 (1967) 1105–1114.

[6] F. Bernardini, H. Rushmeier, The 3D model acquisition pipeline, Computer Graphics Forum 21 (2) (2002) 149–172.

[7] S. Tominaga, N. Tanaka, Estimating reflection parameters from a single color image, IEEE Computer Graphics and Applications 20 (5) (2000) 58–66.

[8] R.T. Tan, K. Nishino, K. Ikeuchi, Separating reflection components based on chromaticity and noise analysis, IEEE Transactions on Pattern Analysis and Machine Intelligence 26 (10) (2004) 1373–1379.

[9] F. Boughorbel, D. Page, C. Dumont, M.A. Abidi, Registration and integration of multi-sensor data for photo-realistic scene reconstruction, in: Applied Imagery Pattern Recognition '99, SPIE, vol. 3905, 1999, pp. 74–84.

[10] P. Dias, V. Sequeira, F. Vaz, J. Goncalves, Registration and fusion of intensity and range data for 3D modelling of real world scenes, in: Proceedings of Fourth International Conference on 3-D Digital Imaging and Modeling, 2003, pp. 418–425.

[11] R. Kurazume, Simultaneous 2d images and 3d geometric model registration for texture mapping utilizing reflectance attribute, in: Proceedings of Fifth Asian Conference on Computer Vision, 2002, pp. 99–106.

[12] P.W. Smith, M.D. Elstrom, Stereo-based registration of range and projective imagery for data fusion and visualization, Optical Engineering 40 (3) (2001) 352–361.

[13] K. Umeda, G. Godin, M. Rioux, Registration of range and color images using gradient constraints and range intensity images, in: Proceedings of 17th International Conference on Pattern Recognition, vol. 3, 2004, pp. 12–15.

[14] K. Umeda, M. Shinozaki, G. Godin, M. Rioux, Correction of color information of a 3D model using a range intensity image, in: Proceedings of Fifth International Conference on 3-D Digital Imaging and Modeling, 2005, pp. 229–236.

[15] M. Shinozaki, K. Umeda, G. Godin, M. Rioux, Correction of intensity of a color image using a range intensity image, in: Proceedings of 18th International Conference on Pattern Recognition, 2006, pp. 774–777.

[16] T.M. Lehmann, C. Palm, Color line search for illuminant estimation in real-world scenes, Journal of the Optical Society of America A 18 (11) (2001) 2679–2691.

[17] J.-A. Beraldin, F. Blais, P. Boulanger, L. Cournoyer, J. Domey, S.F. El-Hakim, G. Godin, M. Rioux, J. Taylor, Real world modelling through high resolution digital 3D imaging of objects and structures, ISPRS Journal of Photogrammetry and Remote Sensing 55 (2000) 230–250.

[18] R. Baribeau, M. Rioux, Influence of speckle on laser range finders, Applied Optics 30 (20) (1991) 2873–2878.

[19] B.K.P. Horn, Robot Vision, MIT Press, 1986.

[20] S.A. Shafer, Using color to separate reflection components, Color Research and Application 10 (1985) 210–218.

[21] L. Piegl, On NURBS: a survey, IEEE Computer Graphics and Applications 11 (1) (1991) 55–71.

[22] ShapeGrabber. Available from: <http://www.shapegrabber.com>.